Energetics and Dynamics of the Reactions of O(^{3}P) with Dimethyl Methylphosphonate and Sarin

Patrick F. Conforti and Matthew Braunstein*

Spectral Sciences, Inc., 4 Fourth Avenue, Burlington, Massachusetts 01803

James A. Dodd

Air Force Research Laboratory/Space Vehicles Directorate, Hanscom Air Force Base, Massachusetts 01731

Received: April 29, 2009; Revised Manuscript Received: September 15, 2009

Electronic structure and molecular dynamics calculations were performed on the reaction systems O(^{3}P) + sarin and O(^{3}P) + dimethyl methylphosphonate (DMMP), a sarin simulant. Transition state geometries, energies, and heats of reaction for the major reaction pathways were determined at several levels of theory, including AM1, B3LYP/6-311+G(d,p), and CBS-QB3. The major reaction pathways for both systems are similar and include H-atom abstraction, H-atom elimination, and methyl elimination, in rough order from low to high energy. The H-atom abstraction channels have fairly low barriers (~10 kcal mol^{-1}) and are close to thermoneutral, while the other channels have relatively high energy barriers (>40 kcal mol^{-1}) and a wide range of reaction enthalpies. We have also found a two-step pathway leading to methyl elimination through O-atom attack on the phosphorus atom for DMMP and sarin. For sarin, the two-step methyl elimination pathway is significantly lower in energy than the single-step pathway. We also present results of O(^{3}P) + sarin and O(^{3}P) + DMMP reaction cross sections over a broad range of collision energies (2−10 km s^{-1} collision velocities) obtained using the direct dynamics method with an AM1 semiempirical potential. These excitation functions are intended as an approximate guide to future hyperthermal measurements, which to our knowledge have not yet examined either of these systems. The reaction barriers, reaction enthalpies, transition state structures, and excitation functions are generally similar for DMMP and sarin, with some moderate differences for methyl elimination energetics, which indicates DMMP will likely be a good substitute for sarin in many O(^{3}P) chemical investigations.

1. Introduction

The proliferation of weapons of mass destruction, especially chemical weapons, has renewed interest in the fundamental chemistry of nerve agents such as sarin, and its simulant dimethyl methylphosphonate (DMMP). Several recent studies have examined the surface chemistry of nerve agents and their simulants, with an emphasis on developing more effective catalytic pathways for their deactivation.[1,2] Similarly, the incineration and combustion chemistry of nerve agents is being investigated to develop methods to more effectively eliminate chemical weapon stockpiles.[3−6] The related chemistry of O(^{3}P) with sarin and DMMP, reported in the present work, is important in assessing the potential chemical interactions following the possible release of nerve agents in the upper atmosphere, where O(^{3}P) can be a significant constituent.

Because there is so little information available on the interaction of O(^{3}P) with sarin and DMMP, it is useful to briefly review recent related sarin and DMMP surface and gas-phase chemistry investigations. Previous studies examined the decomposition of sarin and DMMP on metal oxide surfaces.[1,7,8] For DMMP, the P═O bond was found to bind to an acidic site on the surface and was followed by the elimination of the methoxy groups. From electronic structure calculations, the adsorption of both sarin and DMMP was observed to be qualitatively similar, with both being energetically favorable.[1] In the gas-phase, complementary experimental and kinetic modeling studies of Korobeinichev et al. and Glaude et al. describe possible decomposition mechanisms for pyrolysis of sarin and several of its simulants.[4,9,10] Through high-level ab initio calculations of methyl phosphonic acid, reaction pathways, transition states, and reaction rate kinetics of combustion and other reaction pathways were assessed by Tester and coworkers.[6] The work of Tester et al. provides insights into the fundamental chemical nature of organophosphorous nerve agents and their simulants. As we shall show, some of these insights, such as differences between P-atom and C-atom reactive sites, carry over to the present O-atom chemistry.

The present work is also related to recent studies of collisions between O(^{3}P) and small organic compounds and carbon-based material surfaces. Experimental and theoretical studies of collisions between hyperthermal oxygen and carbon-based surfaces have shown that in addition to the inelastic scattering of O atoms, both C−C bond cleavage and hydrogen abstraction are important processes.[11−15] Studies of collisions between hyperthermal oxygen and small alkanes have shown similar chemistry: the expected OH formation is observed along with hydrogen atom elimination and C−C bond cleavage.[16−19] In these reactions, it was observed that H abstraction to form OH has a barrier of ~5−10 kcal mol^{-1}. The H-atom elimination and C−C bond break reactions, however, had larger barriers (40−50 kcal mol^{-1}). The picture emerging from these studies is that OH formation dominates at low collision energies while H-elimination and to a lesser extent C−C bond cleavage reactions are competitive at higher energies.

* Corresponding author, matthew.braunstein@spectral.com.

10.1021/jp903961b CCC: $40.75
Published on Web 10/30/2009

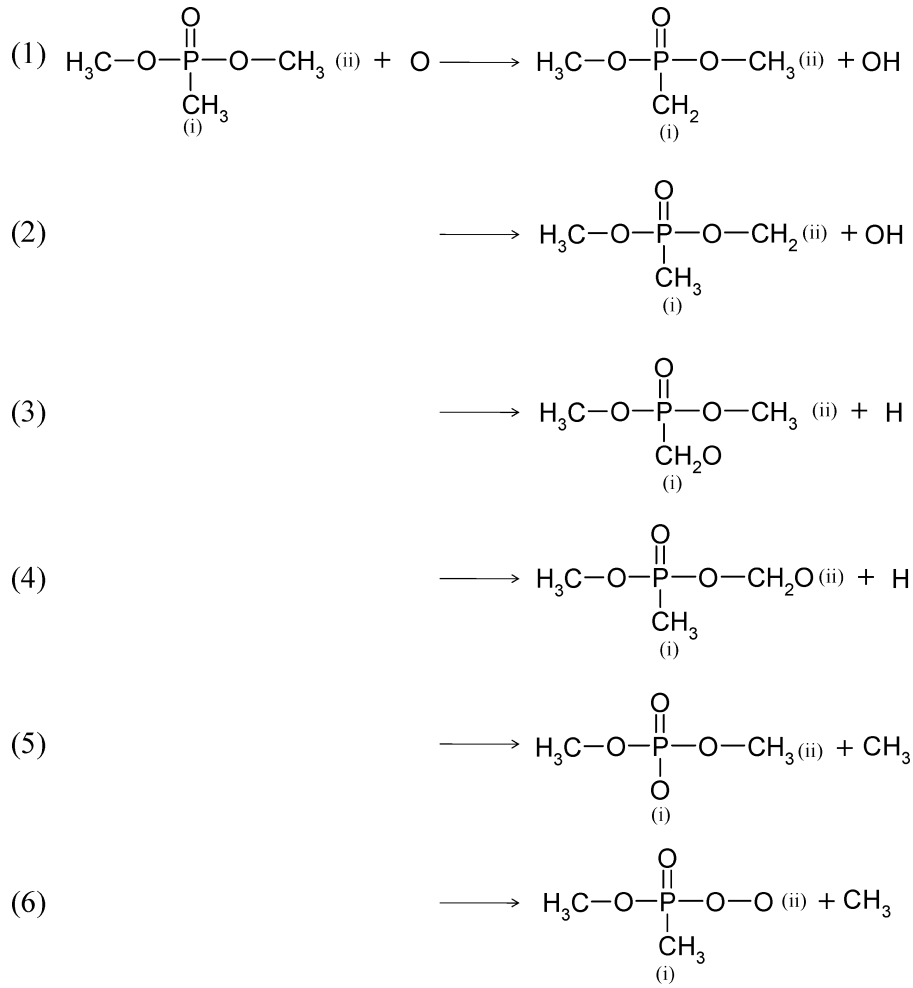

Figure 1. The molecular structure of DMMP and the calculated hydrogen abstraction (1–2), hydrogen elimination (3–4), and methyl elimination (5–6) reaction schemes. The abstraction and elimination sites on each of the molecules are denoted.

In this paper, we describe electronic structure and molecular dynamics calculations on the O(3P) + DMMP and O(3P) + sarin systems. This study focuses on the most significant reactions of hyperthermal O(3P) with DMMP and sarin as are possible in the upper atmosphere. These reactions are shown in Figures 1 and 2 for DMMP and sarin, respectively. Reactions 1 and 2 are H-atom abstraction of DMMP from two different methyl sites, labeled (i) and (ii), to form OH. Reactions 3 and 4 are H-atom elimination of DMMP from the two sites. Finally, reactions 5 and 6 are methyl elimination of DMMP from the two sites. For sarin, H-atom abstraction (7−9) and H-atom elimination (10−12) are investigated at three different sites. Methyl elimination (13−14) is investigated at two different sites. It should be noted that methyl elimination can occur through O(3P) attack on a carbon (14), oxygen (6), or phosphorus (5, 13) atom. While these reactions are not inclusive of all possible reactions, they include the most probable pathways following oxygen collision. Transition state geometries, energies, and heats of reaction for reaction pathways 1−14 were found at the AM1, B3LYP/6-311+G(d,p), and CBS-QB3 levels of theory, except for reaction 5 which was treated at the MP2 and CBS-Q levels as discussed more fully later. Only the lowest triplet states are examined.

We find that the major reaction pathways for both DMMP and sarin are similar. The H-atom abstraction channels have fairly low barriers (∼5−10 kcal mol^{-1}) and are close to thermoneutral. For the most part, the other channels have relatively high energy barriers (>40 kcal mol^{-1}) with a wide range of reaction enthalpies. These reaction features are similar to those discussed above for several O(3P) plus hydrocarbon systems.[17−19] In addition, we have also found a two-step pathway for methyl elimination in both sarin and DMMP, which occurs through O(3P) attack on the phosphorus atom. The highest barrier for the two-step methyl elimination reaction of sarin is 16.6 kcal mol^{-1}, which is significantly lower than single step elimination. Unlike the other reaction channels, there are notable differences between sarin and DMMP for methyl elimination energetics, as we will show later. In addition to the electronic structure calculations, we have also performed direct dynamics simulations, using the AM1 semiempirical potential. From these simulations, we obtained cross sections (excitation functions) for the major reaction channels for the O(3P) + sarin and O(3P) + DMMP reactions over a broad range of collision energies, corresponding to 2−10 km s^{-1} collision velocities. The excitation functions for the two systems are found to be similar. We find that the H-atom abstraction channel dominates at low collision velocities (<7 km/s). H-atom elimination and to a lesser extent methyl elimination becomes competitive at higher collision velocities (>7 km/s), again following the general features of analogous O(3P) + hydrocarbon studies. The excitation functions obtained in this way should serve as an approximate guide to future O(3P) hyperthermal measurements and as a baseline for future calculations with improved potentials. To our knowledge, the present work is the first to examine the chemistry of O(3P) + sarin and O(3P) + DMMP.

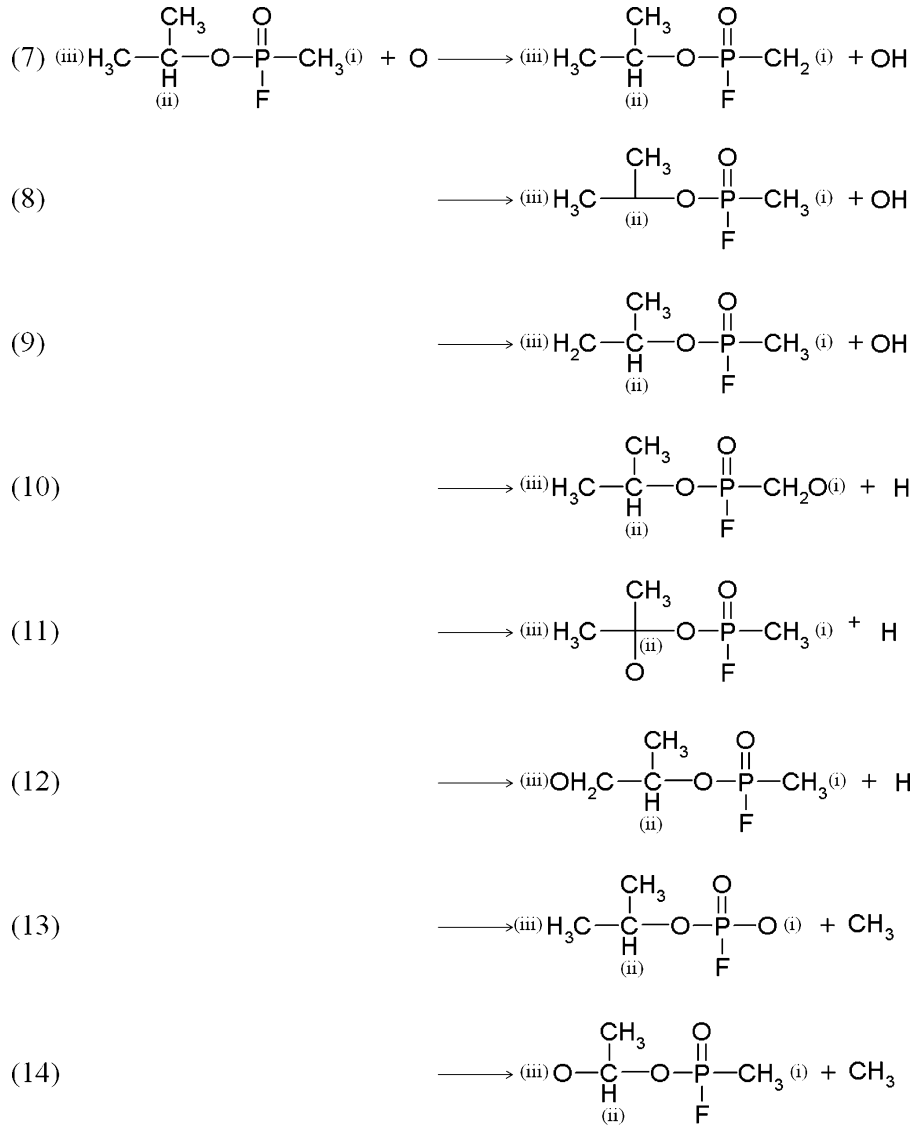

Figure 2. The molecular structure of sarin and the calculated hydrogen abstraction (7–9), hydrogen elimination (10–12), and methyl elimination (13–14) reaction schemes. The abstraction and elimination sites on each of the molecules are denoted.

In section 2, we describe and discuss the results of our electronic structure calculations, and in section 3 we discuss our molecular dynamics calculations. In section 4, we give our conclusions.

2. Electronic Structure Calculations

Stationary points and transition structures for the $O(^3P)$ + sarin and $O(^3P)$ + DMMP systems are calculated at three levels of electronic theory for all reactions except reaction 5: the AM1 semiempirical method,[20] the density functional method B3LYP/6-311+G(d,p),[21−24] and the hybrid CBS-QB3 method.[25] In the case of reaction 5, we had difficulty converging the density functional theory and used instead an MP2 method (MP2/6-311+G(d,p)) and hybrid CBS-Q.[26] The AM1 calculations are performed using GAMESS[27] while the other higher level calculations are performed using the Gaussian03 computational chemistry package.[28] As a point of comparison, calculations of DMMP and sarin absorption on an Al_2O_3 surface gave accurate vibrational spectra results with the B3LYP levels of theory,[1] and calculations using the CBS-Q methods gave exceptional results for the heats of formation of methyl phosphonic acid and its decomposition products.[6] Transition state structures are identified in the present calculations with one imaginary vibrational mode and through intrinsic reaction coordinate calculations. All energies are calculated relative to the reactant asymptote and include zero-point energy corrections. All calculations are performed on the lowest triplet potential energy surface.

2.1. $O(^3P)$ + DMMP. We calculated the barriers ($\Delta E^{\ddagger}$) and reaction enthalpies (ΔE) for the major reaction channels for $O(^3P)$ + DMMP, which include hydrogen abstraction, hydrogen elimination, and methyl elimination reactions. The results at each level of theory are given in Table 1 relative to the $O(^3P)$ + DMMP reactant state. For each of the hydrogen abstraction and elimination reactions, we calculate the barriers and reaction enthalpies from two locations on DMMP as labeled in Figure 1. Reactions at the two $O-CH_3$ sites of DMMP are not exactly equivalent. However, differences in the energetics of the two sites are small, less than 1 kcal mol^{-1}, and therefore only one set of values is reported here. While no available experimental measurements are available for such reactions, as a reference, experimental values of reaction enthalpies for the O + ethane reaction products are −1.8, 8.3, and 0.69 kcal mol^{-1} for the hydrogen abstraction, hydrogen elimination, and methyl elimination reactions, respectively.[17,29] We consider the CBS-QB3

TABLE 1: The Reaction Barriers ($\Delta E^{\ddagger}$) and Enthalpies (ΔE) (in kcal mol^{-1}) of the DMMP + O(^{3}P) Reactions Studied at 0 K[c]

	reaction	$\Delta E^{\ddagger}$ AM1	$\Delta E^{\ddagger}$ DFT/MP2[a]	$\Delta E^{\ddagger}$ CBS-QB3[b]	ΔE AM1	ΔE DFT/MP2[a]	ΔE CBS-QB3[b]
	H abstraction						
(1)	O + $C_3H_9O_3P$ → OH + $C_3H_8O_3P$(i)	18.1	6.6	8.2	−23.3	1.0	0.6
(2)	O + $C_3H_9O_3P$ → OH + $C_3H_8O_3P$(ii)	11.4	5.6	3.2	−32.0	−1.2	−4.3
	H elimination						
(3)	O + $C_3H_9O_3P$ → H + $C_3H_8O_4P$(i)	46.6	59.6	44.2	4.5	32.7	14.2
(4)	O + $C_3H_9O_3P$ → H + $C_3H_8O_4P$(ii)	34.1	49.0	41.0	−13.2	17.9	−2.0
	methyl elimination						
(5)	O + $C_3H_9O_3P$ → Int → CH_3 + $C_2H_6O_4P$(i)	26.2/4.6	50.8/27.6	69.4/9.0	−1.6/−24.0	26.3/−3.4	6.8/−14.22
(6)	O + $C_3H_9O_3P$ → CH_3 + $C_2H_6O_4P$(ii)	60.7	46.6	44.8	25.7	36.6	34.2

[a] Density function theory (B3LYP) is used to calculate the energetics of reactions 1−4 and reaction 6. MP2 is used for reaction 5 with the zero-point energies calculated using HF/6-31G(d′). [b] The hybrid method CBS-QB3 is used to calculate the energetics of reactions 1−4 and reaction 6. CBS-Q is used for reaction 5. [c] For reaction 5, reaction barriers are given for each of the two transition states, and enthalpies are given for the stable intermediate and final product.

and CBS-Q methods to be the most accurate level of theory, and we will use the CBS-QB3 and CBS-Q results here and in future discussion, unless explicitly stated otherwise. Transition state structures are shown in Figure 3, and the full geometries are available online as Supporting Information. Many of the DMMP reaction products shown in Figure 1 have not been previously investigated, and therefore we have calculated the thermochemistry for each species and give these in Table 2.

The hydrogen abstraction reaction pathways have the lowest activation barriers, and therefore OH can be formed at relatively low collision velocities (<4 km s^{-1}). We note that the AM1 energy barriers are in rough agreement with the CBS-QB3 and CBS-Q barriers. For the hydrogen abstraction reactions, a larger activation barrier is computed for reaction 1 with the abstraction occurring at the P−CH_3 site versus at the O−CH_3 in reaction 2. This difference is due to the slight difference in the C−H bond strength at each location on the DMMP molecule. For either reaction 1 or 2, the transition state structure contains an almost linear angle of abstraction between the C−H−O atoms as shown in parts a and b of Figure 3. A large majority of the DMMP molecular structure remains unchanged as the CH_2 radical is formed. The enthalpies of the H-abstraction reactions using AM1 are greatly underpredicted (−23.3 and −32.0 kcal mol^{-1}) compared to the nearly thermoneutral CBS-QB3 results of 0.6 and −4.3 kcal mol^{-1} for reactions 1 and 2, respectively. The CBS-QB3 results are consistent with the reaction enthalpies seen for analogous O(^{3}P) + hydrocarbon H-abstraction reactions. The calculated activation barriers for the H-atom elimination reactions are higher than the hydrogen abstraction reactions by approximately 30−40 kcal mol^{-1}. Additionally, the hydrogen elimination reactions are more endothermic than the abstraction reactions at each level of theory studied. The elimination reaction (4) requires less energy than reaction 3, similar to the abstraction reaction mentioned above. In the saddle points shown in parts c and d of Figure 3, a trigonal bipyramidal structure is observed at the elimination point with the bonding O and the H-atom eliminating on the axial plane. While reaction 3 has more of a S_N2-like transition geometry, Figure 3c, the axial O−C−H bond angle is slightly bent more for reaction 4, Figure 3d. The products of reaction 4 are thermodynamically more stable than reaction 3, with a reaction enthalpy of −2.0 versus 14.2 kcal mol^{-1}.

For the methyl elimination reaction, both a two-step and single-step pathway are calculated. The two-step reaction is determined for CH_3 elimination from position (i) of DMMP, reaction 5. In this reactive channel, the O-atom first attacks the phosphorus as shown in Figure 3e. Then a stable intermediate is formed, as shown in Figure 3f. The energy barrier is calculated to be 69.4 kcal mol^{-1} for this step, and the formation of the intermediate is endothermic. In the second step, the P−C bond breaks and the methyl radical is eliminated. For this step, there is a much smaller barrier of 2.2 kcal mol^{-1} with respect to the intermediate complex. The overall reaction is exothermic with an enthalpy of −14.2 kcal mol^{-1}. The calculated energy barrier for the methyl elimination reaction from position (ii) of DMMP (reaction 6) is smaller than the first step of the two-step reaction. Additionally, the one-step barrier for CH_3 elimination is greater than H-atom abstraction or elimination. More energy is required for the one-step methyl elimination compared with the H-atom elimination as the C−H bond strength for the case of the hydrogen elimination is weaker than the C−C bond. The elimination of the methyl group at site (ii) is endothermic by 34.2 kcal mol^{-1}, in contrast to the elimination at site (i), which is exothermic. For this set of methyl elimination reactions, we must note the large differences between the AM1 results and the CBS results. In particular using the AM1 potential, the barrier for the formation of the intermediate in reaction 5 is approximately 43 kcal/mol less than the CBS calculation, and the barrier for reaction 6 is 16 kcal/mol greater than the CBS calculation. The impact of these energetic differences on the dynamics and reactive cross sections will be discussed in section 3.

2.2. O(^{3}P) + Sarin. Similar to O(^{3}P) + DMMP reactions energetics, we calculate the reaction energies and activation barriers for the hydrogen abstraction reaction, the hydrogen elimination reaction, and the methyl elimination reaction for sarin. The results for the O(^{3}P) + sarin reactions are given in Table 3. All energies are relative to the O(^{3}P) + sarin reactant state. There are two enantiomers of sarin, and only one is considered here, (*R*)-sarin. As opposed to DMMP, we calculate hydrogen abstraction and elimination reactions from three unique sites on the sarin molecule, as shown in Figure 2. Additionally, we calculate the methyl elimination reaction from two sarin sites, one attached to the phosphorus (site (i) of the sarin molecule in Figure 2) and one of the isopropyl methyls (site (iii) of sarin). The transition structures are shown in Figure 4 and the full geometries are available online as Supporting Information. Additionally, the calculated thermochemistry for each of the sarin reaction products shown in Figure 2 is given in Table 4.

The hydrogen abstraction reactions from the O(^{3}P) + sarin require the least amount of energy. The activation barriers range from ∼5 to 10 kcal mol^{-1}, which are all accessible at collision velocities less than 4 km s^{-1}. The abstraction reaction (7), from the methyl attached to the phosphorus atom, has a higher barrier

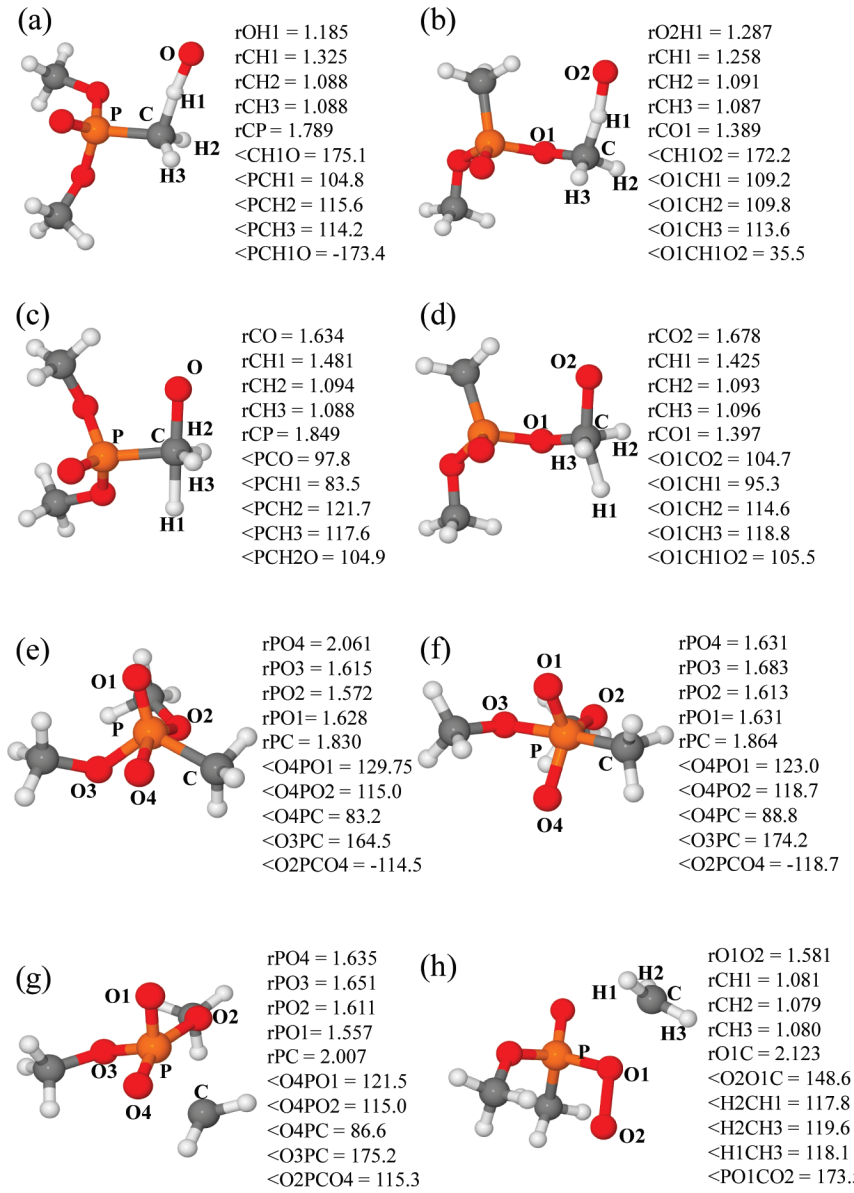

Figure 3. Structures for O(^{3}P) + DMMP, (a) hydrogen abstraction reaction (1) transition state, (b) hydrogen abstraction reaction (2) transition state, (c) hydrogen elimination reaction (3) transition state, (d) hydrogen elimination reaction (4) transition state, (e) methyl elimination reaction (5) first transition state, (f) methyl elimination reaction (5) stable intermediate, (g) methyl elimination reaction (5) second transition state, and (h) methyl elimination reaction (6) transition state. All bond angles (in degrees) and lengths (in angstroms) are from the CBS-QB3 (a–d,h) and CBS-Q (e–g) calculations. Complete geometric information for these transition states is given in the Supporting Information.

TABLE 2: Thermochemistry for DMMP and Its Reactive Products Computed at the CBS-QB3 Level[a]

molecule	E (0 K)	$\Delta_f H$ (0 K)	$\Delta_f H$ (298 K)	S (298 K)
$C_3H_9O_3P$	−685.9038	−197.0	−204.4	0.09652
$C_3H_8O_3P$(i)	−685.2408	−146.2	−152.6	0.09858
$C_3H_8O_3P$(ii)	−685.2485	−151.1	−157.5	0.09719
$C_3H_8O_4P$(i)	−760.3722	−177.5	−184.6	0.1012
$C_3H_8O_4P$(ii)	−760.3891	−188.1	−195.3	0.1011
$C_2H_6O_4P$(i)	−721.1768	−193.2	−198.9	0.09547
$C_2H_6O_4P$(ii)	−721.0921	−140.0	−145.7	0.09478

[a] E is given in hartree molecule^{-1}, $\Delta_f H$ (0 K) and $\Delta_f H$ (298 K) are given in kcal mol^{-1}, and S is given in kcal mol^{-1} K^{-1}.

than reactions 8 and 9, which are relatively close in value. The geometries for the H-abstraction reactions are shown in Figure 4a−c. The C−H−O bond is nearly linear in each case (172−176°). The reaction enthalpies for abstraction range from −5.0 to 2.2 kcal mol^{-1}, with the most exothermic reaction following abstraction from the main chain carbon.

The elimination of hydrogen from sarin requires approximately 30−40 kcal mol^{-1} more energy than the sarin H-atom abstraction reaction. For the H-atom elimination from sites (i) and (ii) of sarin, the transition states proceed through a linear arrangement of the atoms involved in the reaction, while the geometry for the elimination from site (iii) is more bent. The molecular geometries for these states are shown in Figure 4d−f. The overall reaction energy for the elimination of hydrogen on sarin is more endothermic than their abstraction counterparts, ranging from −0.9 to 17.1 kcal mol^{-1}. Similar to the hydrogen abstraction reaction, the hydrogen elimination from position (ii) of sarin, as shown in Figure 2, is the most exothermic reaction, when the main chain carbon is involved in the reaction.

The energetics of the elimination of the methyl group from sites (i) and (iii) of sarin have been calculated. Similar to the CH_3 elimination from DMMP, there are two pathways: a two-step pathway with the methyl group eliminated from the phosphorus (reaction 13), and a high-energy, single-step process

TABLE 3: The Reaction Barriers ($\Delta E^{\ddagger}$) and Enthalpies (ΔE) (in kcal mol^{-1}) of the Sarin + O(^{3}P) Reactions Studied at 0 K[a]

	reaction	$\Delta E^{\ddagger}$ AM1	$\Delta E^{\ddagger}$ DFT	$\Delta E^{\ddagger}$ CBS-QB3	ΔE AM1	ΔE DFT	ΔE CBS-QB3
	H abstraction						
(7)	$O + C_4H_{10}FO_2P \rightarrow OH + C_4H_9FO_2P$(i)	16.7	17.7	10.9	−21.4	15.0	2.2
(8)	$O + C_4H_{10}FO_2P \rightarrow OH + C_4H_9FO_2P$(ii)	13.3	5.5	4.5	−34.2	4.7	−5.0
(9)	$O + C_4H_{10}FO_2P \rightarrow OH + C_4H_9FO_2P$(iii)	12.8	16.8	4.3	−24.4	11.1	0.8
	H elimination						
(10)	$O + C_4H_{10}FO_2P \rightarrow H + C_4H_9FO_3P$(i)	48.2	59.0	47.1	1.5	34.4	17.1
(11)	$O + C_4H_{10}FO_2P \rightarrow H + C_4H_9FO_3P$(ii)	58.9	67.1	53.0	−4.6	18.1	−0.9
(12)	$O + C_4H_{10}FO_2P \rightarrow H + C_4H_9FO_3P$(iii)	42.0	64.9	51.9	−4.1	26.5	10.2
	methyl elimination						
(13)	$O + C_4H_{10}FO_2P \rightarrow Int \rightarrow CH_3 + C_3H_7FO_3P$(i)	12.3/11.0	15.8/12.5	16.6/16.2	1.2/−20.8	3.3/−14.8	7.7/−13.0
(14)	$O + C_4H_{10}FO_2P \rightarrow CH_3 + C_3H_7FO_3P$(iii)	52.7	46.0	60.3	−29.3	−13.6	−7.7

[a] For reaction 13, reaction barriers are given for each of the two transition states, and enthalpies are given for the stable intermediate and final product.

eliminating one of the isopropyl methyl groups (reaction 14). The first saddle point, the stable intermediate, and the second point for the two-step pathway are shown in Figure 4g−i. In the first step, the reaction barrier is 16.6 kcal mol^{-1} and the formation of the intermediate is slightly endothermic (7.7 kcal mol^{-1}). The geometry of the intermediate state is trigonal bipyramidal about the phosphorus. From the intermediate, the reaction barrier is 8.5 kcal mol^{-1} to reach the final product state, which is exothermic by −13.0 kcal mol^{-1}. The activation barrier for the methyl elimination reaction (14) is 60.3 kcal mol^{-1} which is much larger than the two-step process. Similar to the H-atom elimination pathway, a collinear orientation is calculated for the C(H$_3$)−C−O bond angle at the saddle point, shown in Figure 4j. This methyl elimination reaction is exothermic by −7.7 kcal mol^{-1}.

2.3. Discussion. On comparison of O(^{3}P) + DMMP and O(^{3}P) + sarin, the transition state geometries, activation barriers, and reaction energies are generally similar for equivalent types of reactions at equivalent points on the molecules, with some notable differences for methyl elimination energetics. The barriers and reaction enthalpies for the H-atom abstraction and H-atom elimination reactions for the two sets are generally within a few kcal mol^{-1} of each other. For methyl elimination, reactions 5 and 13, there is a difference of ∼50 kcal mol^{-1} in the first barrier of the two-step mechanism. For reactions 6 and 14 there is a ∼15 kcal mol^{-1} difference in the barriers and a ∼40 kcal mol^{-1} difference in the reaction enthalpies. This enthalpy difference between (6) and (14) can be understood by simple bond energy arguments: taking typical *average* bond enthalpy values, for DMMP a rough calculation results in (C−O bond broken) − (O−O bond formed) = 85 − 35 = ∼50 kcal mol^{-1}, and for sarin the estimation is (C−C bond broken) − (C−O bond formed) = 83 − 85 = ∼−2 kcal mol^{-1}. Notwithstanding this, our results show DMMP will probably be a very good simulant for sarin in examining O(^{3}P) atom chemistry for many applications. We note that the methyl elimination pathway from the phosphorus atom in sarin describes a lower energy, two-step pathway which could compete with the other low-energy processes that may occur following an O-atom attack. We further note that based on previous studies,[6] the present CBS-QB3 and CBS-Q results are expected to be benchmark calculations for the O(^{3}P) + DMMP and the O(^{3}P) + sarin systems. In this particular study we focus on the most significant reactive pathways with O(^{3}P) and DMMP or sarin as we are interested in those reactions that could occur with the CWA in the upper atmosphere. In particular, we have not included other reactive pathways, such as cleavage of the P−F bond in sarin which might be important in detoxification reactions. The calculated pathways for this study were determined from preliminary direct dynamics calculations using high-velocity N_2 (nonreactive) and O(^{3}P), and no pathways were observed with P−F bond cleavage following collisions. This observation is consistent with the literature wherein approximate bond energies of P−O, P−C, and P−F are 65, 91, and 117 kcal mol^{-1}, respectively.[30] The large P−F bond energy makes breaking the P−F bond an extremely minor channel.

Finally, we note that although the reaction barriers generally agree within 3−16 kcal/mol between the AM1 level of theory and CBS-QB3 (with the caveat of reaction 5 as discussed in section 2.1), the reaction enthalpies calculated with AM1 are generally too exothermic by a significant amount. For example, for the hydrogen abstraction reaction (1), the AM1 reaction energy is 23.9 kcal mol^{-1} more exothermic than the CBS-QB3 result. Previous calculations of similar abstraction and elimination reactions of hydrocarbons have shown the same trends.[17] Additionally, deviations are observed between the B3LYP and CBS-QB3 values. While we are still investigating the source of these errors in this particular molecular set, absolute maximum errors for the G2 chemistry set using a comparable level of theory have been calculated greater than 30 kcal mol^{-1}.[31] Therefore, future calculations of reaction pathways for DMMP and sarin should be limited to higher level methods such as the CBS.

3. Dynamics Simulations

Molecular dynamics simulations of O(^{3}P) + DMMP and O(^{3}P) + sarin collisions are performed using the dynamic reaction path (DRC) routine[32] within the GAMESS computational chemistry package. The potential is calculated as the simulation progresses using the AM1 semiempirical method, which is computationally tractable for these systems. While AM1 significantly overpredicts reaction enthalpies, stationary point geometries and reaction barriers are generally within 15 kcal mol^{-1} of the CBS values for a majority of the reactive pathways. Total excitation functions should therefore serve as a rough guide to future measurements and modeling.[16] Planned future studies using AM1 with specific reaction parameters, AM1-SRP, will build on this initial effort. The integration time step was 0.1 fs, the initial separation between fragments was set to 15 Å and the final separation to 18 Å, the SCF convergence criterion was set to 1.0×10^{-5} hartree, and the maximum tolerance for the deviation for energy conservation (per step) is set to 5.0×10^{-5} hartree. Collision velocities of 2−10 km s^{-1} are used in this study in order encompass the appropriate range of high-energy collisions that are possible in

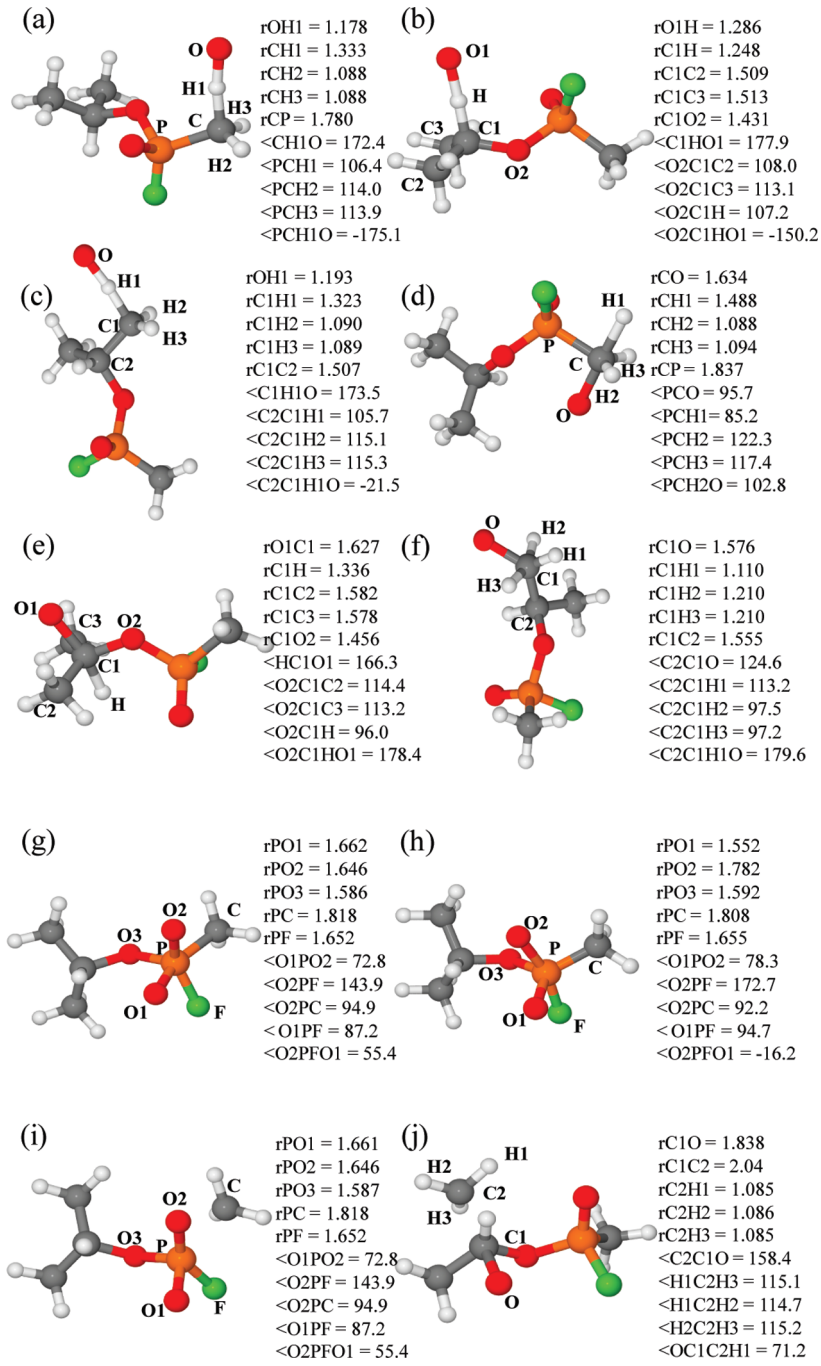

Figure 4. Structures for O(^{3}P) + sarin: (a) hydrogen abstraction reaction (7) transition state, (b) hydrogen abstraction reaction (8) transition state, (c) hydrogen abstraction reaction (9) transition state, (d) hydrogen elimination reaction (10) transition state, (e) hydrogen elimination reaction (11) transition state, (f) hydrogen elimination reaction (12) transition state, (g) methyl elimination reaction (13) first transition state, (h) methyl elimination reaction (13) stable intermediate, (i) methyl elimination reaction (13) second transition state, and (j) methyl elimination reaction (14) transition state. All bond angles (in degrees) and lengths (in angstroms) are from the CBS-QB3 calculations. Complete geometric information for these transition states is given in the Supporting Information.

the upper atmosphere and from molecular beam experiments. We restrict this study to adiabatic dynamics, and only the ground-state triplet surface is used. This is a reasonable approximation as a recent nonadiabatic dynamics study by Schatz and co-workers shows that at hyperthermal collision velocities reactions on the ground state potential surface dominate in approximately a 7:3 ratio.[33] At each collision velocity, 10000 trajectories are performed between each pair of species. In each trajectory, the minimum energy structures of DMMP and sarin are randomly oriented using Euler angles and a random impact parameter is chosen following the procedure of Hase et al.[34] Initial velocities are determined from zero-point energies (normal-mode sampling) and the collision energy studied. The maximum impact parameter is set at 4.1 Å for O + DMMP and 5.0 Å for O + sarin. Most of the trajectories are only run for several hundred femtoseconds to 1 ps to assess the primary collision interaction process and the resulting reaction products. In the following discussion, like reactive channels from different molecular sites are added together to obtain cross sections for each major pathway, i.e., hydrogen abstraction, hydrogen elimination, and methyl elimination.

The reactive cross sections (total excitation functions) are shown as a function of collision velocity (and collision energy) in Figure 5a,b for DMMP and sarin, respectively. The reactive

TABLE 4: Thermochemistry for Sarin and Its Reactive Products at the CBS-QB3 Level[a]

molecule	E (0 K)	$\Delta_f H$ (0 K)	$\Delta_f H$ (298 K)	S (298 K)
$C_4H_{10}FO_2P$	−749.1921	−234.0	−242.4	0.1004
$C_4H_9FO_2P$(i)	−748.5265	−181.6	−188.8	0.1039
$C_4H_9FO_2P$(ii)	−748.5379	−188.8	−196.0	0.1034
$C_4H_9FO_2P$(iii)	−748.5288	−183.1	−190.2	0.1039
$C_4H_9FO_3P$(i)	−823.6527	−209.6	−217.5	0.1078
$C_4H_9FO_3P$(ii)	−823.6813	−227.6	−235.5	0.1043
$C_4H_9FO_3P$(iii)	−823.6636	−216.5	−224.3	0.1073
$C_3H_7FO_3P$(i)	−784.4556	−224.3	−230.9	0.1009
$C_3H_7FO_3P$(iii)	−784.4473	−219.0	−225.6	0.09971

[a] E is given in hartree molecule^{-1}, $\Delta_f H$ (0 K) and $\Delta_f H$ (298 K) are given in kcal mol^{-1}, and S is given in kcal mol^{-1} K^{-1}.

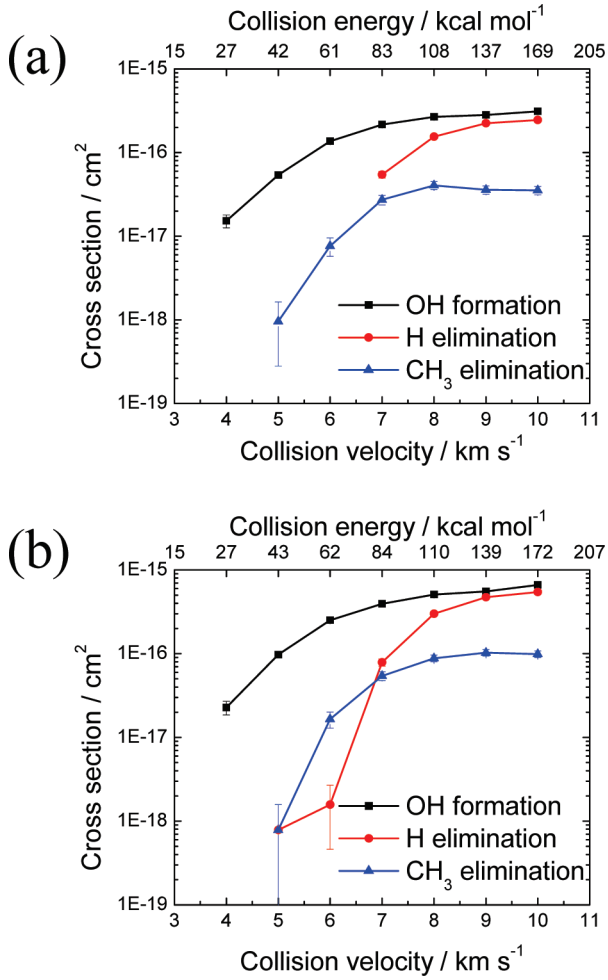

Figure 5. Reactive cross sections given in cm^2 plotted as a function of collision velocity in km s^{-1} and energy in kcal mol^{-1} for (a) O(3P) + DMMP and (b) O(3P) + sarin. The cross sections for OH abstraction (squares), H elimination (circles), and methyl elimination (triangles) are each denoted. In (b), less than 10 reactions are observed for H elimination reactions at 5 and 6 km s^{-1}.

cross sections for DMMP and sarin are similar. The OH formation is present in significant fractions starting at a collision velocity of 4 km s^{-1}, which is ~27 kcal mol^{-1} of collision energy for both the O(3P) + DMMP and O(3P) + sarin systems. As discussed in the previous section, the hydrogen abstraction reaction requires the least amount of energy to form, 11−18 kcal mol^{-1} using the AM1 level of theory. A noticeable number of methyl elimination reactions are observed at 5 km s^{-1} for O(3P) + sarin and O(3P) + DMMP. For sarin, this energy threshold is apparently below the needed energy for the direct "high barrier" elimination channel, and so could indicate that the low-energy, two-step process is occurring. We note, however, that for these classical calculations, reagent zero-point energy could be used to overcome the barrier. While there is a nonzero cross section for the hydrogen elimination reaction of sarin at 5 and 6 km s^{-1}, less than 10 reactions (out of 10000 trajectories) are observed in the simulations and therefore this value has a large degree of uncertainty. A significant cross section for hydrogen elimination begins at 7 km s^{-1} for both O(3P) + DMMP and O(3P) + sarin. For O(3P) + DMMP, the product branching ratios at 8 km s^{-1} are 58:33:9 for OH formation, H elimination, and CH_3 elimination, respectively. For O(3P) + sarin at 8 km s^{-1} the branching ratios are 57:33:10, respectively. The branching ratios between DMMP and sarin are therefore very similar, with OH formation dominating. The H-elimination reaction is a competitive second, and CH_3 elimination is least but still significant. Though, due to the small activation barrier of the DMMP methyl elimination reaction using AM1, the cross section for this particular channel is most likely overestimated at low velocities for O + DMMP. These branching ratios are qualitatively similar to those observed for comparable processes in O(3P) + ethane and propane reactions at 8 km s^{-1}.[16] While the pathways to eliminating the H-atom versus the methyl are energetically competitive, there are approximately three times more sites for hydrogen elimination which probably accounts for much of the difference in the branching ratios between the hydrogen and methyl elimination channels. Additionally, we note that a small number of other reaction products, such as those small molecules resulting from collision-induced dissociation of the main chain O−C and O−P bonds, are observed in the simulations at high velocities. A greater number of trajectories are needed for these reactions to be appropriately analyzed.

As shown in the electronic structure calculations, two pathways for methyl elimination are apparent. However, we have not decomposed the methyl elimination cross section into finer detail to distinguish the branching ratios for these channels. The low number of total methyl elimination reactions (less than 100 out of 10000 at the highest collision velocity tested, 10 km s^{-1}) makes the statistical significance of these partial cross sections insufficient for presentation and discussion in this work. Furthermore as discussed in section 2.1, the approximate nature of the AM1 potential, particularly the energetics and detailed ordering of the barriers for the methyl elimination reaction, would likely lead to inaccuracies for these kinds of detailed cross sections. To account for possible errors, an investigation of the cross sections examined using direct dynamics with an AM1-SRP potential is currently underway. While a detailed account of the methyl elimination reaction is not yet possible, preliminary results indicate that the cross section for the hydrogen abstraction reaction of DMMP using the AM1-SRP is within a factor of 2 of the AM1 results at 8 and 10 km s^{-1}.

Further understanding of the hyperthermal collision process is provided by studying the angular distribution of the products. In Figures 6 and 7, the normalized differential cross sections of the scattering angles are given for each of the H abstraction (a), H elimination (b), and methyl elimination (c) reactions for DMMP and sarin, respectively, using collision velocities of 5, 7, and 10 km s^{-1}. For both DMMP and sarin, the OH is observed to preferentially forward scatter (i.e., scatter in the same direction as the incoming oxygen was traveling) at the higher collision velocities of 7 and 10 km s^{-1}. In previous studies of hyperthermal oxygen collisions with small hydrocarbons and surfaces, the forward scatter of the OH was also observed at high

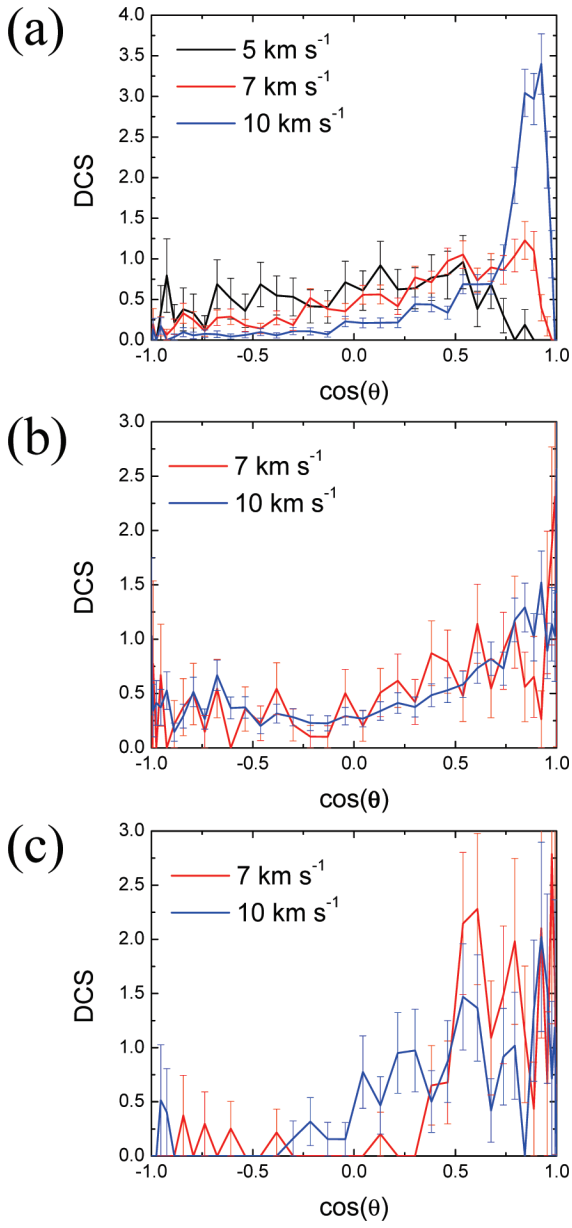

Figure 6. The angular distributions of the scattering products of the $O(^3P)$ + DMMP reaction plotted as normalized differential cross sections, (DCS = $1/\sigma\ d\sigma/(\sin\theta\ d\theta)$, $d\theta = 5°$), at 5, 7, and 10 km s^{-1}: (a) hydrogen abstraction, (b) hydrogen elimination, and (c) methyl elimination. The scattering angle θ is defined as the angle between the incident O atom and the OH, H, or CH_3 product, respectively, in the center-of-mass frame.

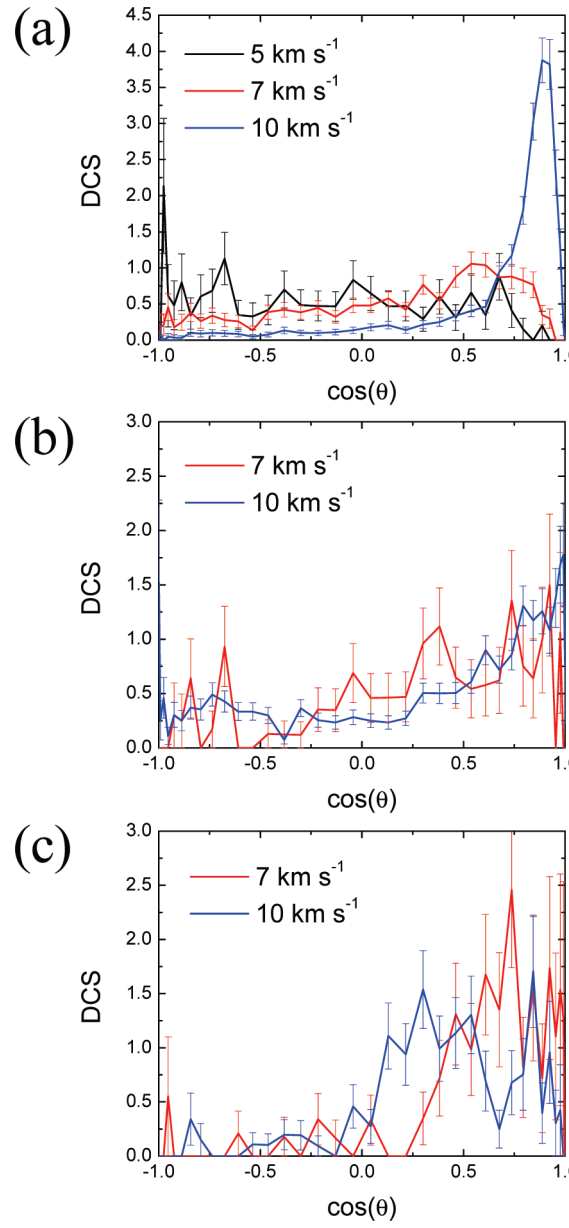

Figure 7. The angular distributions of the scattering products of the $O(^3P)$ + sarin reaction plotted as normalized differential cross sections, (DCS = $1/\sigma\ d\sigma/(\sin\theta\ d\theta)$, $d\theta = 5°$), at 5, 7, and 10 km s^{-1}: (a) hydrogen abstraction, (b) hydrogen elimination, and (c) methyl elimination. The scattering angle θ is defined as the angle between the incident O atom and the OH, H, or CH_3 product, respectively, in the center-of-mass frame.

velocities (a "stripping mechanism") and was attributed to a near linear transition state structure.[11,17,19,35] The same linear arrangement of the atoms involved in the abstraction reaction is calculated for the DMMP and sarin transition structures, and not surprisingly the process dominates here. At the 5 km s^{-1} collision velocity, there is a broad distribution of deflection angles, as the stripping mechanism becomes less effective. Because of large statistical scatter at 5 km s^{-1}, only the 7 and 10 km s^{-1} velocities are plotted for the H and CH_3 elimination reaction. For the hydrogen elimination reactions, the scattering also tends toward forward scattering. As described in the previous sections, the atomic arrangements for the H elimination transition state geometries are nearly linear or slightly bent about the reactive carbon center. The eliminating hydrogen leaves the reactive carbon site in a continuation of the direction of the attacking oxygen. A distribution of scattering angles between 0 and 90° is present as shown in the plots as the collision energy is partitioned between the DMMP or sarin and hydrogen species. For the methyl elimination reactions, the products are observed to scatter at angles of approximately 36−90° at the collision velocities shown in Figures 6 and 7. As discussed in section 2, the methyl-elimination processes occur through bent transition state geometries. Although we have not yet found the relative contributions of the low-energy barrier two-step and high-energy barrier one-step elimination reactions to the totals shown here, we note that the bent transition state geometries in both the single-step and the second step of the two-step methyl elimination processes are consistent with scattering in the side directions, as the CH_3 group leaves following the O-atom attack. Finally, we note that previous simulations ascribe a broad

distribution of scattering angles to a long-lived intermediate species.[19] However, in our simulations at the collision velocities tested, such a distribution is not observed. Future studies will examine individual trajectories to probe the details of such dynamic events.

4. Conclusions

We have used electronic structure and molecular dynamics simulations to explore the chemistry of collisions of atomic oxygen with DMMP and sarin. The electronic structure calculations determined reaction energetics and transition state geometries of three reaction processes: hydrogen abstraction reaction to form OH, hydrogen elimination, and methyl elimination. The reactions were studied at several levels of theory, including AM1, DFT-B3LYP, and CBS-QB3. The hydrogen abstraction reaction was found to require the least amount of energy ($\sim$4−11 kcal mol^{-1} barriers), while the elimination reactions had >40 kcal mol^{-1} barriers at the CBS-QB3 level. We have also found a two-step pathway for methyl elimination through O-atom attack on the phosphorus atom, which for sarin reactions could compete with the other low-energy processes following an O-atom attack. Generally, the reaction barriers, reaction enthalpies, and transition state structures are similar for DMMP and sarin, with the exception of methyl elimination where barriers and enthalpies showed some notable differences. Cross sections (excitation functions) were determined using direct dynamics at the AM1 level. While AM1 consistently overestimated reaction exothermicities, the activation barriers were, with the exception of reaction 5, within 16 kcal mol^{-1} of the CBS-QB3 calculations. For both DMMP and sarin, the reactive cross sections are similar as a function of collision velocity with the hydrogen abstraction reaction channel dominating, and the H, and CH_3 elimination becoming competitive at collision velocities >7 km s^{-1}. The branching ratios for H-atom abstraction, H-elimination, and methyl elimination at 8 km s^{-1} were found to be similar to like processes in O(^{3}P)-atom reactions with small hydrocarbons, roughly 60:30:10, respectively. The scattering cross sections for the reaction products for DMMP and sarin were found to be similar for like processes and revealed a qualitative description of the interaction processes. For many applications, therefore, DMMP will likely be a good substitute for sarin for O(^{3}P) atom chemical investigations.

Future work will focus on improving the AM1 semiempirical potential surface with specific reaction parameters (SRPs), for use in dynamics studies. More detailed examinations will then be performed, including investigations of product internal energies, comparisons of the relative reactivity of different atomic sites, and investigations of the relative contributions of the two-step versus one-step methyl elimination pathways.

Acknowledgment. This work was supported by a DTRA/JSTO basic research program award, BRCALL07-N-2-0029. M.B. and P.F.C. acknowledge support under Contract No. FA8718-05-C-0077. We would like to thank R. Dressler for his comments on the manuscript.

Supporting Information Available: Geometries of all optimized structures from Figures 1−4. This material is available free of charge via the Internet at http://pubs.acs.org.

References and Notes

(1) Bermudez, V. M. *J. Phys. Chem. C* **2007**, *111*, 9314.
(2) Bermudez, V. M. *J. Phys. Chem. C* **2009**, *113*, 1917.
(3) Yang, Y. C.; Baker, J. A.; Ward, J. R. *Chem. Rev.* **1992**, *92*, 1729.
(4) Glaude, P. A.; Curran, H. J.; Pitz, W. J.; Westbrook, C. K. *Proc. Combust. Inst.* **2000**, *28*, 1749.
(5) Korobeinichev, O. P.; Shvartsberg, V. M.; Shmakov, A. G.; Bolshova, T. A.; Jayaweera, T. M.; Melius, C. F.; Pitz, W. J.; Westbrook, C. K.; Curran, H. J. *Proc. Combust. Inst.* **2005**, *30*, 2353.
(6) Sullivan, P. A.; Sumathi, R.; Green, W. H.; Tester, E. W. *Phys. Chem. Chem. Phys.* **2004**, *6*, 4296.
(7) Mitchell, M. B.; Sheinker, V. N.; Mintz, E. A. *J. Phys. Chem. B* **1997**, *101*, 11192.
(8) Sheinker, V. N.; Mitchell, M. B. *Chem. Mater.* **2002**, *14*, 1257.
(9) Korobeinichev, O. P.; Ilyin, S. B.; Bolshova, T. A.; Shvartsberg, V. M.; Chernov, A. A. *Combust. Flame* **2000**, *121*, 593.
(10) Glaude, P. A.; Melius, C.; Pitz, W. J.; Westbrook, C. K. *Proc. Combust. Inst.* **2002**, *29*, 2469.
(11) Zhang, J. M.; Garton, D. J.; Minton, T. K. *J. Chem. Phys.* **2002**, *117*, 6239.
(12) Zhang, J. M.; Upadhyaya, H. P.; Brunsvold, A. L.; Minton, T. K. *J. Phys. Chem. B* **2006**, *110*, 12500.
(13) Nicholson, K. T.; Minton, T. K.; Sibener, S. J. *J. Phys. Chem. B* **2005**, *109*, 8476.
(14) Troya, D.; Schatz, G. C. *J. Chem. Phys.* **2004**, *120*, 7696.
(15) Kim, D.; Schatz, G. C. *J. Phys. Chem. A* **2007**, *111*, 5019.
(16) Garton, D. J.; Minton, T. K.; Troya, D.; Pascual, R.; Schatz, G. C. *J. Phys. Chem. A* **2003**, *107*, 4583.
(17) Troya, D.; Pascual, R. Z.; Garton, D. J.; Minton, T. K.; Schatz, G. C. *J. Phys. Chem. A* **2003**, *107*, 7161.
(18) Troya, D.; Pascual, R. Z.; Schatz, G. C. *J. Phys. Chem. A* **2003**, *107*, 10497.
(19) Yan, T. Y.; Doubleday, C.; Hase, W. L. *J. Phys. Chem. A* **2004**, *108*, 9863.
(20) Dewar, M. J. S.; Zoebisch, E. G.; Healy, E. F.; Stewart, J. J. P. *J. Am. Chem. Soc.* **1985**, *107*, 3902.
(21) Becke, A. D. *J. Chem. Phys.* **1993**, *98*, 5648.
(22) Lee, C. T.; Yang, W. T.; Parr, R. G. *Phys. Rev. B* **1988**, *37*, 785.
(23) Vosko, S.; Wilk, L.; Nusair, M. *Can. J. Phys.* **1980**, *58*, 1200.
(24) Stephens, P. J.; Devlin, F. J.; Chabalowski, C. F.; Frisch, M. J. *J. Phys. Chem.* **1994**, *98*, 11623.
(25) Montgomery, J. A.; Frisch, M. J.; Ochterski, J. W.; Petersson, G. A. *J. Chem. Phys.* **1999**, *110*, 2822.
(26) Ochterski, J. W.; Petersson, G. A. J. A.; Montgomery, J. *J. Chem. Phys.* **1996**, *104*, 2598.
(27) Schmidt, M. W.; Baldridge, K. K.; Boatz, J. A.; Elbert, S. T.; Gordon, M. S.; Jensen, J. H.; Koseki, S.; Matsunaga, N.; Nguyen, K. A.; Su, S. J.; Windus, T. L.; Dupuis, M.; Montgomery, J. A. *J. Comput. Chem.* **1993**, *14*, 1347.
(28) Frisch, M. J.; Trucks, G. W.; Schlegel, H. B.; Scuseria, G. E.; Robb, M. A.; Cheeseman, J. R.; Montgomery J. A., Jr.; Vreven, T.; Kudin, K. N.; Burant, J. C.; Millam, J. M.; Iyengar, S. S.; Tomasi, J.; Barone, V.; Mennucci, B.; Cossi, M.; Scalmani, G.; Rega, N.; Petersson, G. A.; Nakatsuji, H.; Hada, M.; Ehara, M.; Toyota, K.; Fukuda, R.; Hasegawa, J.; Ishida, M.; Nakajima, T.; Honda, Y.; Kitao, O.; Nakai, H.; Klene, M.; Li, X.; Knox, J. E.; Hratchian, H. P.; Cross, J. B.; Bakken, V.; Adamo, C.; Jaramillo, J.; Gomperts, R.; Stratmann, R. E.; Yazyev, O.; Austin, A. J.; Cammi, R.; Pomelli, C.; Ochterski, J. W.; Ayala, P. Y.; Morokuma, K.; Voth, G. A.; Salvador, P.; Dannenberg, J. J.; Zakrzewski, V. G.; Dapprich, S.; Daniels, A. D.; Strain, M. C.; Farkas, O.; Malick, D. K.; Rabuck, A. D.; Raghavachari, K.; Foresman, J. B.; Ortiz, J. V.; Cui, Q.; Baboul, A. G.; Clifford, S.; Cioslowski, J.; Stefanov, B. B.; Liu, G.; Liashenko, A.; Piskorz, P.; Komaromi, I.; Martin, R. L.; Fox, D. J.; Keith, T.; Al-Laham, M. A.; Peng, C. Y.; Nanayakkara, A.; Challacombe, M.; Gill, P. M. W.; Johnson, B.; Chen, W.; Wong, M. W.; Gonzalez, C.; Pople, J. A. *Gaussian 03, Revision C.02*; Gaussian, Inc.: Wallingford, CT, 2003.
(29) Sander, S.; Friedl, R.; Ravishankara, A.; Golden, D.; Kolb, C.; Kurylo, M.; Molina, M.; Moortgat, G.; Keller-Rudek, H.; Finlayson-Pitts, B.; Wine, P.; Huie, R.; Orkin, V. *Chemical Kinetics and Photochemical Data for Use in Atmospheric Studies*; JPL Publication 06-2, 2006.
(30) Goldwhite, H. *Introduction to Phosphorus Chemistry*; Cambridge University Press: Cambridge, 1981.
(31) Foresman, J. B.; Frisch, A. *Exploring Chemistry with Electronic Structure Methods*, 2nd ed.; Gaussian, Inc.: Pittsburgh, PA, 1996.
(32) Taketsugu, T.; Gordon, M. S. *J. Chem. Phys.* **1995**, *103*, 10042.
(33) Hu, W.; Lendvay, G.; Maiti, B.; Schatz, G. C. *J. Phys. Chem. A* **2008**, *112*, 2093.
(34) Hase, W. L.; Ludlow, D.; Wolf, R.; Schlick, T. *J. Phys. Chem.* **1981**, *85*, 958.
(35) Polanyi, J. C. *Acc. Chem. Res.* **1972**, *5*, 161.

JP903961B